Environmental Science & Technology

pubs.acs.org/est

Article

AQDS and Redox-Active NOM Enables Microbial Fe(III)-Mineral Reduction at cm-Scales

Yuge Bai, Adrian Mellage, Olaf A. Cirpka, Tianran Sun, Largus T. Angenent, Stefan B. Haderlein, and Andreas Kappler*

Cite This: *Environ. Sci. Technol.* 2020, 54, 4131−4139

Read Online

ACCESS | Metrics & More | Article Recommendations | Supporting Information

ABSTRACT: Redox-active organic molecules such as anthraquinone-2,6-disulfonate (AQDS) and natural organic matter (NOM) can act as electron shuttles thus facilitating electron transfer from Fe(III)-reducing bacteria (FeRB) to terminal electron acceptors such as Fe(III) minerals. In this research, we examined the length scale over which this electron shuttling can occur. We present results from agar-solidified experimental incubations, containing either AQDS or NOM, where FeRB were physically separated from ferrihydrite or goethite by 2 cm. Iron speciation and concentration measurements coupled to a diffusion-reaction model highlighted clearly Fe(III) reduction in the presence of electron shuttles, independent of the type of FeRB. Based on our fitted model, the rate of ferrihydrite reduction increased from 0.07 to 0.19 μmol d^{-1} with a 10-fold increase in the AQDS concentration, highlighting a dependence of the reduction rate on the electron-shuttle concentration. To capture the kinetics of Fe(II) production, the effective AQDS diffusion coefficient had to be increased by a factor of 9.4. Thus, we postulate that the 2 cm electron transfer was enabled by a combination of AQDS molecular diffusion and an electron hopping contribution from reduced to oxidized AQDS molecules. Our results demonstrate that AQDS and NOM can drive microbial Fe(III) reduction across 2 cm distances and shed light on the electron transfer process in natural anoxic environments.

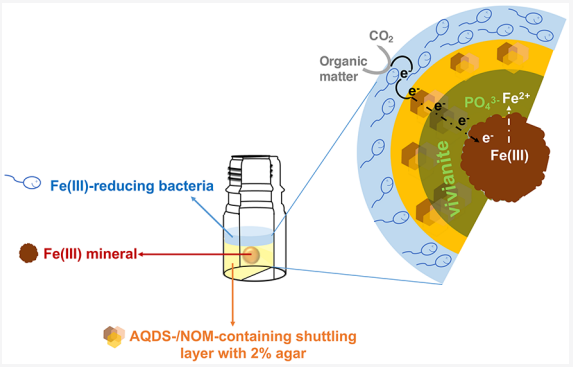

INTRODUCTION

Fe(III) (oxyhydr)oxides are crucial mineral phases involved in major biogeochemical cycles in sediments and soils. Under anoxic conditions, dissimilatory Fe(III)-reducing bacteria (FeRB) can use Fe(III) minerals as terminal electron acceptors for respiration.[1,2] Microbial reduction of Fe(III) minerals such as ferrihydrite or goethite results in their dissolution and thus in the release of sorbed or incorporated compounds such as arsenic or phosphate. The dissolved Fe(II) produced can reprecipitate forming new Fe(II)-bearing minerals such as magnetite, siderite, or vivianite, depending on the rate of Fe(II) formation, pH, temperature, and the presence of other geochemical species.[3,4] These processes can affect the environmental fate of toxic metals, radionuclides, and organic contaminants.[5−8]

Under neutral pH conditions, Fe(III) minerals exist as poorly soluble phases that cannot be taken up into cells for microbial respiration. While microbes can reside directly on Fe(III) mineral surfaces, they have also adapted strategies to access solid-phase electrons when separated from the mineral phase. FeRB can rely on extracellular electron transfer, rather than direct cell contact, to reduce Fe(III) minerals.[9] Different mechanisms for extracellular electron transfer at nanometer (nm) to micrometer (μm) separations have been reported. Among these are the formation of *c*-type-cytochrome-containing pili and nanowires,[10−13] the excretion of Fe(III) chelators to induce the solubilization of Fe(III) minerals to use the dissolved Fe(III) as the electron acceptor,[14] electron hopping via redox-active cofactors that are present in a biofilm,[15] or the usage of electron shuttles between FeRB and Fe(III) minerals.[9]

Electron transfer by electron shuttles from FeRB to Fe(III) minerals involves two reaction steps. First, FeRB donate electrons to the shuttle, the reduced electron shuttle subsequently transports the electrons (either by diffusion of the shuttle or by electron hopping) toward the Fe(III) mineral where it then transfers electrons abiotically, getting oxidized and transported back to the FeRB thus resetting the sequence.[16] To be recyclable, the electron shuttle compound must contain redox-active functional groups, such as a quinone/hydroquinone moiety. A model quinone compound

Received: November 25, 2019
Revised: February 10, 2020
Accepted: February 28, 2020
Published: February 28, 2020

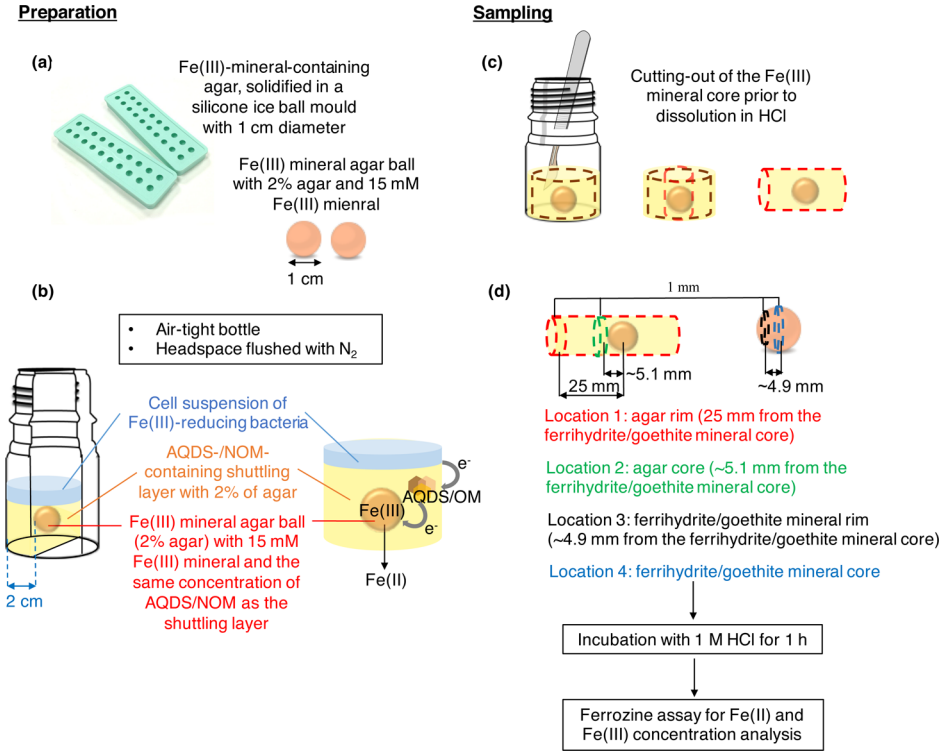

Figure 1. Preparation and sampling of agar-solidified electron shuttling experimental setup. (a) Fe(III) mineral agar ball was prepared in a silicone mould with 1 cm diameter. (b) core was located in the middle of an air-tight 100 mL glass bottle, surrounded by the AQDS- or NOM-containing shuttling layer. The suspension of Fe(III)-reducing bacteria (FeRB) was added on top of the agar with 2 cm distance from the Fe(III) mineral. The headspace of all setups was flushed with N_2 and the setups were incubated at 30 °C in dark. (c) For sampling, a 1 cm diameter core was taken from the center of the agar containing the Fe(III) mineral core. (d) Four pieces of agar with an approximate thickness of 1 mm were sampled at different locations in the core.

that has been widely used in electron-shuttling studies is anthraquinone-2,6-disulfonate (AQDS). Additional shuttling compounds include flavins (excreted by some FeRB), dissolved and solid-phase humic substances, biochar particles, and natural organic matter (NOM).[17−21] Previous studies demonstrated that electron shuttling can facilitate microbial Fe(III) reduction over μm distances.[22,23] However, in the environment, the spatial separation between the FeRB and Fe(III) minerals can be out of the μm range and whether electron shuttling can also happen over longer distances, for example, over centimeters (cm), has remained unknown until now.

In this study, we incubated the FeRB (*Shewanella oneidensis* MR-1 or *Geobacter sulfurreducens*) separated from Fe(III) minerals (ferrihydrite or goethite) by 2 cm in the presence of shuttling compounds. We also collected geochemical data and coupled them to reactive transport modeling to probe separation distance, shuttle type, and shuttle concentration as controls modulating extracellular Fe(III) mineral reduction. Our findings shed new light on the feasibility and mechanisms of extracellular electron transfer, as a driver of Fe(III) mineral reduction, in natural anoxic environments.

MATERIALS AND METHODS

Agar-Solidified Reactors. All preparation steps were performed under sterile conditions. To prepare the shuttling layer with AQDS or organic matter [OM, including Pahokee Peat humic acid (PPHA) and Suwannee River NOM (SRNOM)], the AQDS or OM solutions were added to the warm autoclaved agar solution (for preparation steps see Section S1 in the Supporting Information) under vigorous shaking. A total of 80 mL of the shuttle-agar mix was poured into a 100 mL bottle in ice water (Figure S1). The Fe(III) mineral agar ball (preparation see Section S1 in the Supporting Information) was dropped into the agar when ~2 cm of the bottom and the side of the agar in the bottle were solidified, but the middle part was still liquid, to fix the Fe(III) mineral agar ball in the center of the agar layer. When the agar was completely solidified, the headspace of the bottle was flushed with N_2 gas, closed with a rubber stopper and a screw cap to make it airtight. A suspension of FeRB (1 mL) and 1 mL of the growth medium, containing either acetate (for *G. sulfurreducens*) or lactate (for *S. oneidensis* MR-1) as an electron donor, were added on top of the agar in the bottle. The cultivation of FeRB, preparation of cell suspensions and AQDS/OM solution, and Fe(III) mineral synthesis are described in the Supporting Information (Sections S2−S4).

Sampling and Geochemical Analyses. Sacrificial sampling was conducted anaerobically by placing triplicate bottles for each setup into a glovebox (100% N_2, with a copper bed for oxygen removal). The overlaying cell suspensions were removed with a pipette. A scalpel was used to cut the edge of the agar until it was small enough to be taken out of the bottle (Figure 1c). A 10 mL syringe, cut at the top, was used to collect the solid agar sample (Figure 1c). A 1 mm thick sample was taken at four different locations from the bottle (Figure 1d), two from the AQDS-/OM-containing shuttling layer, one that was at the interface with the overlaying cell suspension (agar rim), and one that was in contact with the Fe(III) mineral agar ball. Two additional samples were taken from the

https://dx.doi.org/10.1021/acs.est.9b07134
Environ. Sci. Technol. 2020, 54, 4131−4139

Fe(III) mineral ball, one that was in contact with the AQDS-/OM-containing shuttling layer (ferrihydrite/goethite rim) and one from the center of the ball (ferrihydrite/goethite). The four agar samples were incubated in a 1 M HCl (for ferrihydrite) or 6 M HCl (for goethite) solution for 1 h. At the end of the extraction, the agar became colorless, indicating the complete dissolution of minerals from the agar to the HCl solution. After 10 min of centrifugation at 13,000 rpm, the Fe(II) and Fe(III) concentration were quantified using the spectrophotometric ferrozine assay in a microtiterplate assay.[24−26]

Diffusion-Reaction Model. We developed a numerical model, simulating reaction coupled to diffusive transport in radial coordinates, to help interpret the measured iron dynamics in the AQDS incubations with ferrihydrite and *S. oneidensis* MR-1. The experimental setup was approximated by a spherical domain, which we justify by the spherical shape of the ferrihydrite agar ball. The model considers that iron geochemistry is driven by abiotic dissimilatory ferrihydrite reduction via the reduced quinone, AH_2QDS and that AH_2QDS is produced via the enzymatically catalyzed oxidation of lactate to acetate (assumed to only occur at the outer edge of the domain, where the cells were situated), coupled to AQDS reduction. The products of ferrihydrite reduction include aqueous Fe^{2+} and solid-bound (adsorbed) Fe(II) and the reduced iron phosphate mineral phase vivianite. We included the precipitation of vivianite because an immobile Fe(II) phase, measured in the experiment, accumulated at the fringe between the ferrihydrite ball and the clean agar. Aqueous Fe^{2+} would have otherwise diffused away from the source. Reactive transport of the dissolved chemical species i within the spherical domain is described by

$$\frac{\partial C_i}{\partial t} = \frac{2D_e}{r}\frac{\partial C_i}{\partial r} + D_e\frac{\partial^2 C_i}{\partial r^2} + R_i$$

in which C_i [mol L^{-1}] is the dissolved concentration of compound i, D_e [m^2 h^{-1}] is the effective diffusion coefficient, accounting for both molecular diffusion and electron hopping, R_i [mol L^{-1} h^{-1}] is the sum of all rates of reactions producing the chemical species minus those consuming it, and r and t are the radial distance and time, respectively. For a detailed description of rate expressions and coefficients that constitute the term R_i, refer to the Supporting Information (Section S5). Transport and reaction were solved jointly, in MATLAB, by applying finite-volume discretization in space and integrating the nonlinear system of ordinary differential equations via the ordinary-differential-equation solver ode15s. The model was fitted to the experimental Fe(II) data using $DREAM_{ZS}$, a Markov-chain Monte Carlo-based (MCMC) method,[27,28] generating parameter distributions, conditioned on the measurements, and subsequent ranges of conditional parameter uncertainty. Model results are presented for the geometric mean value of the fitted parameter distributions (see the Supporting Information, Table S2, for calibrated parameter values and uncertainty ranges). The root mean square error was <0.67 mM for all AQDS-treatments.

RESULTS AND DISCUSSION

AQDS-Mediated Ferrihydrite Reduction. Using an agar-solidified experimental setup, *S. oneidensis* MR-1 was spatially separated from the ferrihydrite-agar ball by 2 cm, with AQDS in the surrounding agar layer as the electron shuttle (Figure 1). Figure 2 presents time series of total Fe(II) and Fe(III) concentrations at different sampling locations (as shown in Figure 1) in the solid agar matrix for the 0.1 mM AQDS treatment inoculated with *S. oneidensis* MR-1. After 5 days of incubation, the Fe(III) concentration at the rim of the ferrihydrite sphere decreased from its starting value of 15 to 4 mM (Figure 2b). Concurrently, Fe(II) accumulated directly outside the ferrihydrite sphere at the sampling location 2 (agar core) until plateauing at 10.3 mM after 15 days of incubation (Figure 2a). No accumulation of Fe(II) was measured in the ferrihydrite core or agar rim (locations 1 and 4). An increase of Fe(II) concentration up to 3 mM and subsequent decrease to 0 mM was measured at the ferrihydrite rim (location 3), after 15 days of incubation (Figure 2a). We attribute the dynamics in location 3 to the sorption of Fe(II) onto ferrihydrite, which over time dissolved and yielded a rerelease of dissolved Fe(II) with the inward progression of the dissolution front. The reductive dissolution of the ferrihydrite was observable from

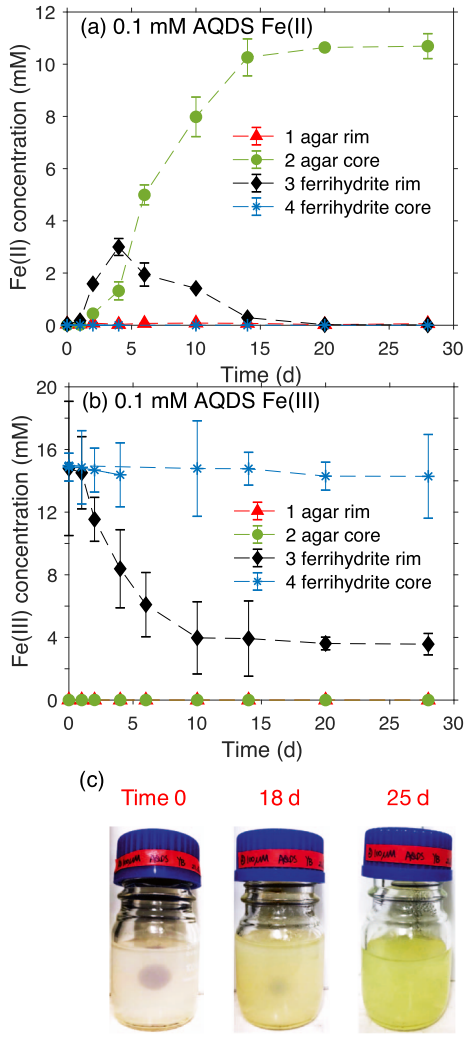

Figure 2. Fe(II) (a) and Fe(III) (b) concentrations measured at four locations of the agar of the microbial reduction experiment with ferrihydrite (15 mM) and *S. oneidensis* MR-1 (10^8 cells mL^{-1}) in the presence of 15 mM lactate as electron donor and 0.1 mM AQDS as electron shuttle. Data are means from triplicate bottles ±standard deviation. (c) Gradual appearance of yellow color in the AQDS layer and the disappearance of the ferrihydrite core in the middle, indicating the progress of microbial Fe(III) reduction over time.

https://dx.doi.org/10.1021/acs.est.9b07134
Environ. Sci. Technol. 2020, 54, 4131−4139

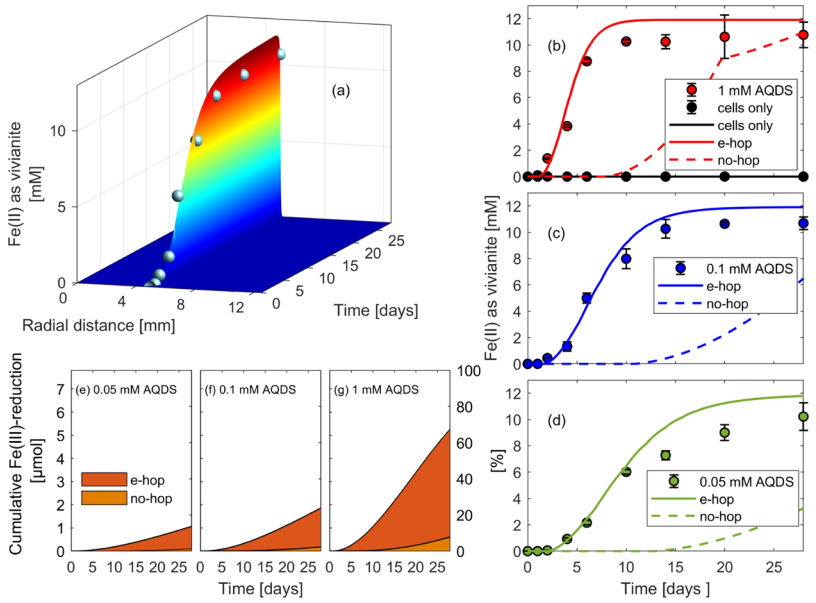

Figure 3. Comparison between measured and simulated concentrations. (a): simulated immobile Fe(II) accumulation, as vivianite, as function of radial distance from the center of the ferrihydrite core and time (surface plot) compared to measured values at the ferrihydrite-agar boundary (between the sampling locations 2 and 3) (spheres), for the 0.1 mM AQDS treatment. (b–d): Comparison between 9.4-fold enhanced AQDS diffusion (e-hop) (solid line) and pure-diffusion (no e-hop) (dashed line) scenarios for Fe(II) production, at 5 mm from the center of the ferrihydrite (location 2, agar core), in all AQDS concentration treatments. (e–g): Computed cumulative Fe(III) reduction is shown for all scenarios.

the color change of the agar (Figure 2c). The Fe(II) produced from the reduction of Fe(III), at the ferrihydrite rim, diffused out to the agar core, but did not further diffuse to the agar rim, instead it accumulated at location 2, the agar core. The available phosphate (from the phosphate buffer used to prepare the AQDS and OM solutions) in the agar likely reacted with the newly reduced Fe(II) to precipitate vivianite, thus resulting in an immobile solid Fe(II) phase. The transformation of ferrihydrite to vivianite in the presence of phosphate buffer has been previously reported in studies with similar concentrations of OM, phosphate buffer, cells, and ferrihydrite.[29−31]

Figure 3 presents a comparison between experimental data and model-predicted vivianite accumulation, along with the model-computed cumulative Fe(III) reduction. The good agreement between the simulated and measured Fe(II) concentrations supports the inclusion of vivianite precipitation in the numerical model, which successfully captured the measured accumulation of an immobile Fe(II) solid phase. Figure S2 of the Supporting Information presents results of a model version without vivianite precipitation, which did not lead to Fe(II) accumulation at location 2 (the agar core), further supporting the inclusion of an immobile Fe(II) phase to fit the measured Fe(II) concentrations. Our Fe concentration measurements suggest a slight spatial separation between the reductive dissolution front at the sampling location 3 (ferrihydrite rim) and the accumulation of vivianite at the location 2 (agar core) (Figure 2a,b), while the model predicts that these would co-occur in closer proximity (data not shown). We attribute this to be an artifact of our sampling procedure which was partly driven by visually observing the boundary of the ferrihydrite-agar ball to the clean agar, and thus subject to slight spatial bias with the progression of the dissolution front. The fitted parameter values and their uncertainty ranges are summarized in the Supporting Information, Table S2. The MCMC-based calibration considerably reduced the prior distribution estimates for each parameter. Briefly, the two parameters controlling the kinetics of ferrihydrite reduction and lactate oxidation, k_{fh} and k_{lac} with calibrated geometric mean values of 5.4×10^4 L mmol^{-1} d^{-1} and 0.11 mmol L^{-1} d^{-1}, exhibited narrow uncertainty ranges: $3.5–8.4 \times 10^4$ L mmol^{-1} d^{-1} and 0.08–0.17 mmol L^{-1} d^{-1}, respectively. The range of uncertainty for k_{lac} lies well within that of previously reported literature values.[32−34] Calibrated parameters with high uncertainty of estimation corresponded to half-saturation (Monod) constants (e.g., K_{lac}) and the rate coefficient for the sorption (k_{sorb}) linear driving force approximation (eq S5 in the Supporting Information, see Table S2). Half-saturation coefficients are difficult to constrain under conditions where their magnitude is smaller than the concentration range of the substrate. Overall, the parameters governing reaction kinetics and transport exhibit low uncertainty of estimation, and the agreement between the numerical model and the experimental data of all three treatments supports our conceptual understanding of the reactive system.

In a recent study, the addition of AQDS enabled the reduction of the Mn(IV) oxide birnessite over a distance of 40 μm, compared to the successful reduction of Mn(IV) oxides over 15 μm in the absence of AQDS by *G. sulfurreducens* with conductive nanowires and cell-excreted Riboflavin as cofactors.[35] Our study, with the amendment of 0.1 mM AQDS, showed the microbial reduction of ferrihydrite that was initially 2 cm away from the microbial cells (Figure 2a). Our control experiments in the agar-solidified setup, amended with only *S. oneidensis* MR-1 or *G. sulfurreducens* (in the absence of electron shuttles), showed no Fe(II) production within 50 days of incubation (Figure S3). Thereby, confirming that shuttling via FeRB-produced flavins, cytochromes, or conductive nanowires cannot shuttle electrons over 2 cm distances, and supporting

https://dx.doi.org/10.1021/acs.est.9b07134
Environ. Sci. Technol. 2020, 54, 4131−4139

AQDS-mediated extracellular reduction. Furthermore, fluorescence microscopy (Figure S4) did not detect the presence of cells in the agar of the AQDS setups throughout the incubation (note: no cells were detected in the agar of the PPHA and SRNOM amended treatments either). The lack of cells in the agar confirms previous reports that the pore size of 2% agar (100−200 nm) is too dense for FeRB to penetrate,[36−38] and thus well-suited to prevent direct cell contact between the cells and the ferrihydrite.

Potential Electron-Transfer Mechanisms. At the upper boundary, where the cells are in contact with the agar, AQDS is reduced to AH_2QDS by *S. oneidensis* MR-1, resulting in a localized drop in the redox potential (E_h) and thus more reducing conditions. Conversely, at the ferrihydrite boundary, the presence of the electron acceptor, Fe(III), reoxidizes the AH_2QDS to AQDS, thus resulting in a relatively higher AQDS/AH_2QDS ratio, and subsequently a more oxidizing E_h. Figure 4 shows the computed E_h for the AQDS/AH_2QDS couple from the simulated AQDS/AH_2QDS concentration ratios, along with the difference in E_h between the upper boundary, in contact with cells, and at the ferrihydrite edge, for the 0.1 mM AQDS concentration treatment. The redox gradient between the more reduced top boundary, in contact with *S. oneidensis* MR-1 cells, and the ferrihydrite yields an electromotive force which drives electrons from the outer edge of the agar to the ferrihydrite (Figure 4).

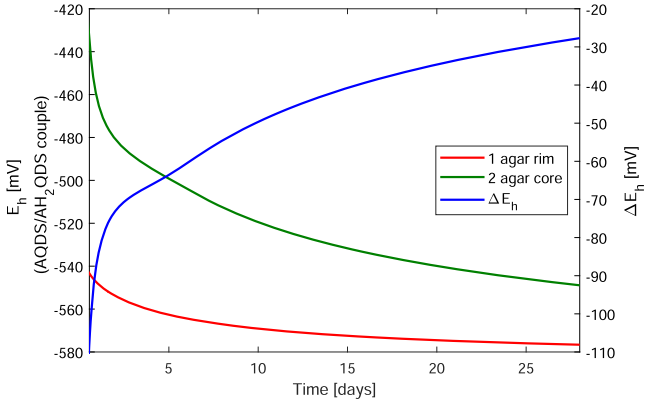

Figure 4. Redox potential (E_h) computed by the diffusion-reaction model for the AQDS/AH_2QDS redox couple, at the agar rim that is in contact with the FeRB (red line) and the agar core, in contact with the ferrihydrite agar ball (green line), for the 0.1 mM AQDS treatment. The reduction potential difference (ΔE_h, blue line) is computed as the difference in E_h between the more reducing agar rim and the more oxidizing agar core, and is the electromotive force driving electrons from the outer edge of the agar to the ferrihydrite. An example calculation of the reduction potential is shown in the Supporting Information, Section S6.

Huskinson et al.[39] and Liao et al.[40] reported an aqueous diffusion coefficient of AQDS of 4.80×10^{-10} m^2 s^{-1}. In our 2% agar medium we measured an effective diffusion coefficient, D_e^{AQDS}, of 5.76 ($\pm$1.46) $\times 10^{-11}$ m^2 s^{-1}, via cyclic voltammetry (for method details see the Supporting Information Section S7), one order of magnitude lower than in water. To capture the timing of Fe(II) accumulation, at location 2 in our experiment, we had to increase the magnitude of D_e^{AQDS} in the reactive-transport model by a calibrated factor (f_{hop}) of 9.41 (uncertainty range: 8.92−9.85). The almost 10-fold higher D_e^{AQDS} suggests the presence of a mechanism which increases the transport flux of reduced quinone, and thus electrons, to the Fe(III) mineral. We propose that this contribution arises from direct electron transfer (electron hopping/self-exchange reaction) between AH_2QDS and AQDS molecules.[41] Figure 3b−d shows a comparison between the model results with electron hopping (e^--hop) and only by molecular diffusion of AQDS (no e-hop). Considering an electron hopping contribution successfully captured the timing of Fe(II) accumulation at location 2 (agar core), as observed in the experiments, without leading to Fe(II) appearing in the ferrihydrite core (sampling location 4), while the "no e-hop" scenario lagged behind for all treatments (Figure 3b−d). (Note: faster lactate oxidation kinetics in the model were unable to capture the timing of Fe(II) accumulation without leading to significant Fe(II) accumulation at the ferrihydrite-core). Our parameterization of enhanced effective diffusion, however, does not account for a dependence on the AQDS concentration. An enhancement factor was chosen as it best fits all three experimental results. Furthermore, it is calibrated for diffusion in an agar solidified medium and should be interpreted as an approximation of a hopping/self-exchange contribution. Further research is needed to more mechanistically parameterize enhanced electron transfer as a function of increasing AQDS concentration.

Considering electron hopping as the dominant electron transfer pathway of AQDS molecules, the simulated cumulative Fe(III) reduction shows that within the 28-day incubation period, 14, 24, and 67% of the Fe(III) was reduced in the 0.05, 0.1, and 1 mM AQDS treatments, respectively (Figure 3e−g). The higher extent of reduction, with increasing AQDS concentration, is a direct result of increased shuttle availability to transport electrons to the ferrihydrite.[23] Because of the reoxidation of AQDS, the model predicts that, with long enough incubation times, each concentration treatment will yield complete reduction of the bioavailable ferrihydrite. However, the overall rate of ferrihydrite reduction (total reduced divided by the incubation time) varies with the AQDS concentration. For an increasing AQDS concentration from 0.05, 0.1, to 1 mM, the ferrihydrite reduction rate increased from 0.04, 0.07, to 0.19 μmol d^{-1}, respectively. With increasing AQDS concentrations, the distance between these molecules is reduced; therefore, the time required for electron hopping is shorter, ultimately resulting in a faster Fe(III) reduction rate. We postulate that electron-carrying AH_2QDS molecules diffuse toward the ferrihydrite core, carrying with them electrons, which in addition, driven by the E_h-gradient, can hop between neighboring AQDS molecules and enhance the flux of the electrons transported to Fe(III).

NOM as an Fe(III)-Reducing Electron Shuttle. Figure 5 shows Fe(II) and Fe(III) concentration time series for agar-solidified incubation experiments with PPHA or SRNOM as the electron shuttle. PPHA amendment resulted in a decrease in the Fe(III) concentration in the ferrihydrite rim from ~15 to 8 mM, within 20 days of incubation (Figure 5b). Concurrently, Fe(II) increased at the agar core from 0 to ~7 mM, and remained stable until the end of the experiment (Figure 5a). The production of Fe(II), mediated by electron transfer over 2 cm, was also found in the setups of ferrihydrite reduction with *G. sulfurreducens* (Figure S5a−d), goethite reduction with *G. sulfurreducens* (Figure S5e−h), or *S. oneidensis* MR-1 (Figure S6), with both PPHA and SRNOM as electron shuttles. In general, goethite was reduced to a much smaller extent compared to ferrihydrite (Figures S5e−h and

https://dx.doi.org/10.1021/acs.est.9b07134
Environ. Sci. Technol. 2020, 54, 4131−4139

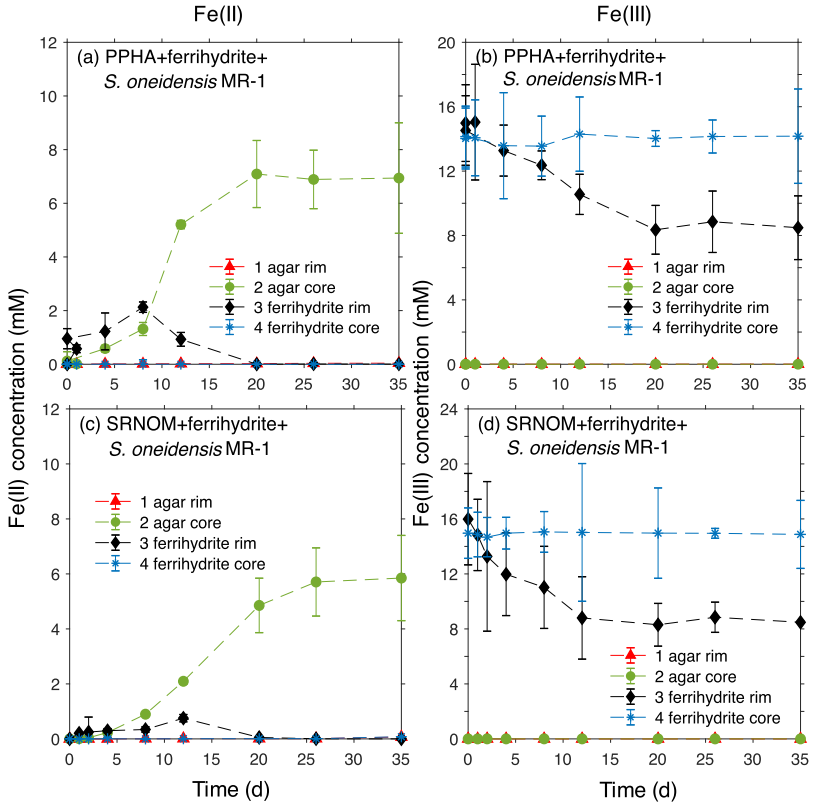

Figure 5. Microbial reduction of 15 mM ferrihydrite by 10^8 cells mL^{-1} of *S. oneidensis* MR-1 in the presence of 15 mM lactate as electron donor, 100 mg L^{-1} PPHA (a,b) or SRNOM (c,d) as electron shuttle. All experiments were conducted with the agar-solidified setup as shown in Figure 1 with 2 cm shuttling distance and incubated at 30 °C in the dark. Data are means from triplicate bottles ±standard deviation, shown as Fe(II) and Fe(III) concentration at four different locations of the agar.

S6) because of the higher crystallinity of goethite than ferrihydrite. Most likely the formation of vivianite also occurred in the OM amended setups, evidenced by the accumulation of immobile Fe(II) in the agar core, and no detection of Fe(II) at the agar rim in all setups (Figure 5a and the Supporting Information S5 and S6).

Because of the lower molecular weight of SRNOM, we would expect a larger diffusion coefficient of SRNOM than PPHA, and thus a larger reduction extent of Fe(III) minerals. However, Figures 5 and S5 and S6 all show that, regardless of the identity of FeRB and Fe(III) mineral, PPHA always yields more Fe(II) for the same incubation time than SNROM. As discussed above, we postulate that the electron transfer pathway between shuttle molecules and the Fe(III) mineral is enhanced via electron hopping; therefore, instead of the molecular size, we expect the amount of quinone functional groups to influence the extent of ferrihydrite reduction. PPHA, with a higher electron accepting capacity,[42] therefore containing more quinone functional groups[42] and more electron hopping sites,[43] can accept more electrons per unit molecule compared to SRNOM, and reduce more Fe(III) mineral within the same time.

Additionally, the lower extent of Fe(III) mineral reduction with SRNOM could also be caused by the more positive reduction potential of SRNOM compared to PPHA, as determined by the mediated electrochemical analysis.[42] At pH 7, the reduction potential of the redox couple FeOOH (synthesized ferrihydrite)-Fe^{2+} is +0.768 V, as measured by mediated potentiometry using a Pt ring combined redox electrode and expressed against the standard hydrogen electrode.[44,45] Therefore, electron shuttles with reduction potentials negative enough (e.g., $E_h^{0\prime}$ of $AQDS_{ox}$−$AQDS_{red}$ is −0.186 V, pH 7) are able to reduce the ferrihydrite after being reduced by the FeRB. Thus, with a more positive reduction potential, reduced SRNOM may reduce ferrihydrite to a lesser extent than reduced PPHA.[46]

In addition to its function as an electron shuttle, NOM can interact with both the Fe(III) minerals and Fe(II) without exchanging electrons. Complexation of Fe(II) by the NOM could have increased the thermodynamic driving force for Fe(III) reduction.[47] However, previous studies have shown that phosphate can outcompete OM for Fe(II),[48] and the formation of vivianite in our experiments further supports that the complexation of Fe(II) by OM did not seem to exert a noticeable influence on the Fe(III) reduction. Moreover, the adsorption of OM to the Fe(III) mineral surfaces could potentially block surface sites[49] and induce aggregation.[50] However, the starting state of the ferrihydrite/goethite agar ball was a ferrihydrite/goethite-OM aggregated agar ball because the same concentration of OM as in the shuttling agar was used in the ferrihydrite/goethite ball. Finally, although OM can act as a ligand promoting Fe(III) solubilization,[14,51,52] the highest Fe(III) concentration found outside the ferrihydrite/goethite agar ball (sampling location 2, see Figure 1) was 0.02 mM, suggesting that the release of Fe(III) via chelation by OM was negligible during our experiment. In summary, we postulate that electron shuttling by OM, that is, OM-facilitated electron transfer between the cells that were physically separated from the ferrihydrite and

https://dx.doi.org/10.1021/acs.est.9b07134
Environ. Sci. Technol. 2020, 54, 4131−4139

goethite was the main mode of action of the added OM in our experiments.

Implications. Batch experiments have typically been used to study the effects of AQDS and OM as electron shuttles on microbial Fe(III) reduction.[19,20,48,50,53−55] However, because of various interactions between OM and Fe(III) minerals, it is challenging to evaluate the extent to which OM stimulates the microbial Fe(III) reduction by acting as an electron shuttle.[48] Our study showed that microbial Fe(III) reduction can occur over 2 cm distance with only AQDS or OM acting as the electron shuttle. Coupling our experimental data with a diffusion-reaction model shed light on an electron hopping contribution (in addition to molecular diffusion) as an electron transfer pathway between AQDS/OM. Although the organic carbon concentration used in our study (100 mg C L^{-1}) was much higher than in most natural settings,[56] our experiment with 0.05 mM AQDS suggest that even a low concentration of redox-active organic molecules could stimulate the microbial reduction of Fe minerals over cm distances. Furthermore, long enough time-scales, would result in the complete reduction of Fe(III) oxides, even at low concentrations of electron shuttles, because of the reversibility of the oxidation/reduction of quinone groups. Additionally, we showed that long-distance electron transfer is independent of the crystallinity of the Fe(III) mineral and the identity of the FeRB and can be facilitated by multiple types of OM.

■ ASSOCIATED CONTENT

Supporting Information

The Supporting Information is available free of charge at https://pubs.acs.org/doi/10.1021/acs.est.9b07134.

Detailed experimental procedures including preparation of agar for the electron shuttling experiment, cultivation of Fe(III)-reducing bacteria, preparation of PPHA and SRNOM solutions, synthesis of Fe(III) minerals, details of the diffusion-reaction model, calculation of the reduction potential (E_h) of AQDS-AH_2QDS redox couple, determination of diffusion coefficient of AQDS in 2% agar by cyclic voltammetry, reactions that happened in the experiment of ferrihydrite reduction by *S. oneidensis* MR-1 with AQDS as electron shuttle, fitted rate coefficients for the diffusion reaction model and their corresponding uncertainty, pictures of the preparation of the agar-solidified experimental setup, simulated mobile Fe(II) concentration with the omission of vivianite formation, Fe(II) concentration over time in the experiments with FeRB only (without electron shuttle), fluorescence microscopy images of the cell suspension solution and in the agar of the experiments amended with AQDS, PPHA, and SRNOM, Fe(II) concentration over time in the experiments of *G. sulfurreducens* reduction of ferrihydrite and goethite with PPHA or SRNOM as electron shuttle, *S. oneidensis* MR-1 reduction of goethite, simulated Fe(II), Fe(III), AQDS, and AH_2QDS concentration for the 0.1 mM AQDS treatment, and the matrix scatter plot visualizing the parameter distribution after calibrating the model (PDF)

■ AUTHOR INFORMATION

Corresponding Author

Andreas Kappler − *Geomicrobiology, Center for Applied Geosciences, University of Tübingen, D-72074 Tübingen, Germany;* orcid.org/0000-0002-3558-9500; Phone: +49-7071-2974992; Email: andreas.kappler@uni-tuebingen.de

Authors

Yuge Bai − *Geomicrobiology, Center for Applied Geosciences, University of Tübingen, D-72074 Tübingen, Germany*

Adrian Mellage − *Hydrogeology, Center for Applied Geosciences, University of Tübingen, D-72074 Tübingen, Germany;* orcid.org/0000-0003-2708-4518

Olaf A. Cirpka − *Hydrogeology, Center for Applied Geosciences, University of Tübingen, D-72074 Tübingen, Germany*

Tianran Sun − *Environmental Biotechnology, Center for Applied Geosciences, University of Tübingen, D-72074 Tübingen, Germany*

Largus T. Angenent − *Environmental Biotechnology, Center for Applied Geosciences, University of Tübingen, D-72074 Tübingen, Germany;* orcid.org/0000-0003-0180-1865

Stefan B. Haderlein − *Environmental Mineralogy and Chemistry, Center for Applied Geosciences, University of Tübingen, D-72074 Tübingen, Germany;* orcid.org/0000-0002-9309-8523

Complete contact information is available at: https://pubs.acs.org/10.1021/acs.est.9b07134

Notes

The authors declare no competing financial interest.

■ ACKNOWLEDGMENTS

This study was supported by a grant from the German Research Foundation (KA1736/37-1). We would like to thank Ellen Roehm for the development of the agar-solidified experimental setup and the preliminary tests. We thank Paula Eisnecker, Ellen Roehm, and Manuel Schad for their help to set up the experiments. Many thanks to Lars Grimm and Franziska Schaedler for their technical support in the laboratory.

■ REFERENCES

(1) Fredrickson, J. K.; Zachara, J. M.; Kennedy, D. W.; Dong, H.; Onstott, T. C.; Hinman, N. W.; Li, S.-m. Biogenic iron mineralization accompanying the dissimilatory reduction of hydrous ferric oxide by a groundwater bacterium. *Geochim. Cosmochim. Acta* **1998**, *62*, 3239−3257.

(2) Nealson, K. H.; Saffarini, D. Iron and manganese in anaerobic respiration - environmental significance, physiology, and regulation. *Annu. Rev. Microbiol.* **1994**, *48*, 311−343.

(3) Coker, V. S.; Gault, A. G.; Pearce, C. I.; van der Laan, G.; Telling, N. D.; Charnock, J. M.; Polya, D. A.; Lloyd, J. R. XAS and XMCD evidence for species-dependent partitioning of arsenic during microbial reduction of ferrihydrite to magnetite. *Environ. Sci. Technol.* **2006**, *40*, 7745−7750.

(4) Hansel, C. M.; Benner, S. G.; Neiss, J.; Dohnalkova, A.; Kukkadapu, R. K.; Fendorf, S. Secondary mineralization pathways induced by dissimilatory iron reduction of ferrihydrite under advective flow. *Geochim. Cosmochim. Acta* **2003**, *67*, 2977−2992.

(5) Gadd, G. M. Microbial influence on metal mobility and application for bioremediation. *Geoderma* **2004**, *122*, 109−119.

(6) Lloyd, J. R.; Sole, V. A.; Van Praagh, C. V. G.; Lovley, D. R. Direct and Fe(II)-mediated reduction of technetium by Fe(III)-reducing bacteria. *Appl. Environ. Microbiol.* **2000**, *66*, 3743−3749.

(7) Newsome, L.; Morris, K.; Lloyd, J. R. The biogeochemistry and bioremediation of uranium and other priority radionuclides. *Chem. Geol.* **2014**, *363*, 164−184.
(8) Watts, M. P.; Coker, V. S.; Parry, S. A.; Pattrick, R. A. D.; Thomas, R. A. P.; Kalin, R.; Lloyd, J. R. Biogenic nano-magnetite and nano-zero valent iron treatment of alkaline Cr(VI) leachate and chromite ore processing residue. *Appl. Geochem.* **2015**, *54*, 27−42.
(9) Glasser, N. R.; Saunders, S. H.; Newman, D. K. The colorful world of extracellular electron shuttles. *Annu. Rev. Microbiol.* **2017**, *71*, 731−751.
(10) Gorby, Y. A.; Yanina, S.; McLean, J. S.; Rosso, K. M.; Moyles, D.; Dohnalkova, A.; Beveridge, T. J.; Chang, I. S.; Kim, B. H.; Kim, K. S.; Culley, D. E.; Reed, S. B.; Romine, M. F.; Saffarini, D. A.; Hill, E. A.; Shi, L.; Elias, D. A.; Kennedy, D. W.; Pinchuk, G.; Watanabe, K.; Ishii, S.; Logan, B.; Nealson, K. H.; Fredrickson, J. K. Electrically conductive bacterial nanowires produced by Shewanella oneidensis strain MR-1 and other microorganisms. *Proc. Natl. Acad. Sci. U.S.A.* **2006**, *103*, 11358−11363.
(11) Lovley, D. R.; Malvankar, N. S. Seeing is believing: novel imaging techniques help clarify microbial nanowire structure and function. *Environ. Microbiol.* **2015**, *17*, 2209−2215.
(12) Speers, A. M.; Schindler, B. D.; Hwang, J.; Genc, A.; Reguera, G. Genetic identification of a PilT motor in Geobacter sulfurreducens reveals a role for pilus retraction in extracellular electron transfer. *Front. Microbiol.* **2016**, *7*, 1578.
(13) Subramanian, P.; Pirbadian, S.; El-Naggar, M. Y.; Jensen, G. J. Ultrastructure of Shewanella oneidensis MR-1 nanowires revealed by electron cryotomography. *Proc. Natl. Acad. Sci. U.S.A.* **2018**, *115*, E3246−E3255.
(14) Nevin, K. P.; Lovley, D. R. Mechanisms for Fe(III) oxide reduction in sedimentary environments. *Geomicrobiol. J.* **2002**, *19*, 141−159.
(15) Snider, R. M.; Strycharz-Glaven, S. M.; Tsoi, S. D.; Erickson, J. S.; Tender, L. M. Long-range electron transport in Geobacter sulfurreducens biofilms is redox gradient-driven. *Proc. Natl. Acad. Sci. U.S.A.* **2012**, *109*, 15467−15472.
(16) Scott, D. T.; McKnight, D. M.; Blunt-Harris, E. L.; Kolesar, S. E.; Lovley, D. R. Quinone moieties act as electron acceptors in the reduction of humic substances by humics-reducing microorganisms. *Environ. Sci. Technol.* **1998**, *32*, 2984−2989.
(17) Marsili, E.; Baron, D. B.; Shikhare, I. D.; Coursolle, D.; Gralnick, J. A.; Bond, D. R. Shewanella secretes flavins that mediate extracellular electron transfer. *Proc. Natl. Acad. Sci. U.S.A.* **2008**, *105*, 3968−3973.
(18) von Canstein, H.; Ogawa, J.; Shimizu, S.; Lloyd, J. R. Secretion of flavins by Shewanella species and their role in extracellular electron transfer. *Appl. Environ. Microbiol.* **2008**, *74*, 615−623.
(19) Lovley, D. R.; Coates, J. D.; Blunt-Harris, E. L.; Phillips, E. J. P.; Woodward, J. C. Humic substances as electron acceptors for microbial respiration. *Nature* **1996**, *382*, 445−448.
(20) Roden, E. E.; Kappler, A.; Bauer, I.; Jiang, J.; Paul, A.; Stoesser, R.; Konishi, H.; Xu, H. Extracellular electron transfer through microbial reduction of solid-phase humic substances. *Nat. Geosci.* **2010**, *3*, 417−421.
(21) Kappler, A.; Wuestner, M. L.; Ruecker, A.; Harter, J.; Halama, M.; Behrens, S. Biochar as an electron shuttle between bacteria and Fe(III) minerals. *Environ. Sci. Technol. Lett.* **2014**, *1*, 339−344.
(22) Lies, D. P.; Hernandez, M. E.; Kappler, A.; Mielke, R. E.; Gralnick, J. A.; Newman, D. K. Shewanella oneidensis MR-1 uses overlapping pathways for iron reduction at a distance and by direct contact under conditions relevant for biofilms. *Appl. Environ. Microbiol.* **2005**, *71*, 4414−4426.
(23) Michelson, K.; Alcalde, R. E.; Sanford, R. A.; Valocchi, A. J.; Werth, C. J. Diffusion-based recycling of flavins allows Shewanella oneidensis MR-1 to yield energy from metal reduction across physical separations. *Environ. Sci. Technol.* **2019**, *53*, 3480−3487.
(24) Hegler, F.; Posth, N. R.; Jiang, J.; Kappler, A. Physiology of phototrophic iron(II)-oxidizing bacteria: implications for modern and ancient environments. *FEMS Microbiol. Ecol.* **2008**, *66*, 250−260.
(25) Stookey, L. L. Ferrozine - a new spectrophotometric reagent for iron. *Anal. Chem.* **1970**, *42*, 779−781.
(26) Viollier, E.; Inglett, P. W.; Hunter, K.; Roychoudhury, A. N.; Van Cappellen, P. The ferrozine method revisited: Fe(II)/Fe(III) determination in natural waters. *Appl. Geochem.* **2000**, *15*, 785−790.
(27) Laloy, E.; Vrugt, J. A. High-dimensional posterior exploration of hydrologic models using mmultiple-try $DREAM_{(ZS)}$ and high-performance computing. *Water Resour. Res.* **2012**, *48*, 1526−1544.
(28) Vrugt, J. A. Markov chain Monte Carlo simulation using the DREAM software package: Theory, concepts, and MATLAB implementation. *Environ. Model. Software* **2016**, *75*, 273−316.
(29) Chen, J.; Gu, B.; Royer, R.; Burgos, W. The roles of natural organic matter in chemical and microbial reduction of ferric iron. *Sci. Total Environ.* **2003**, *307*, 167−178.
(30) Piepenbrock, A.; Dippon, U.; Porsch, K.; Appel, E.; Kappler, A. Dependence of microbial magnetite formation on humic substance and ferrihydrite concentrations. *Geochim. Cosmochim. Acta* **2011**, *75*, 6844−6858.
(31) Shimizu, M.; Zhou, J.; Schröder, C.; Obst, M.; Kappler, A.; Borch, T. Dissimilatory reduction and transformation of ferrihydrite-humic acid coprecipitates. *Environ. Sci. Technol.* **2013**, *47*, 13375−13384.
(32) Bonneville, S.; Van Cappellen, P.; Behrends, T. Microbial reduction of iron(III) oxyhydroxides: effects of mineral solubility and availability. *Chem. Geol.* **2004**, *212*, 255−268.
(33) Mellage, A.; Smeaton, C. M.; Furman, A.; Atekwana, E. A.; Rezanezhad, F.; Van Cappellen, P. Linking spectral induced polarization (SIP) and subsurface microbial processes: Results from sand column incubation experiments. *Environ. Sci. Technol.* **2018**, *52*, 2081−2090.
(34) Roden, E. E. Fe(III) oxide reactivity toward biological versus chemical reduction. *Environ. Sci. Technol.* **2003**, *37*, 1319−1324.
(35) Michelson, K.; Sanford, R. A.; Valocchi, A. J.; Werth, C. J. Nanowires of Geobacter sulfurreducens require redox cofactors to reduce metals in pore spaces too small for cell passage. *Environ. Sci. Technol.* **2017**, *51*, 11660−11668.
(36) Caccavo, F.; Lonergan, D. J.; Lovley, D. R.; Davis, M.; Stolz, J. F.; Mcinerney, M. J. Geobacter sulfurreducens sp. nov., a hydrogen- and acetate-oxidizing dissimilatory metal-reducing microorganism. *Appl. Environ. Microbiol.* **1994**, *60*, 3752−3759.
(37) Hau, H. H.; Gralnick, J. A. Ecology and biotechnology of the genus Shewanella. *Annu. Rev. Microbiol.* **2007**, *61*, 237−258.
(38) Narayanan, J.; Xiong, J.-Y.; Liu, X.-Y. Determination of agarose gel pore size: Absorbance measurements vis other techniques. *J. Phys. Conf.* **2006**, *28*, 83−86.
(39) Huskinson, B.; Marshak, M. P.; Suh, C.; Er, S.; Gerhardt, M. R.; Galvin, C. J.; Chen, X.; Aspuru-Guzik, A.; Gordon, R. G.; Aziz, M. J. A metal-free organic-inorganic aqueous flow battery. *Nature* **2014**, *505*, 195−198.
(40) Liao, S.; Zong, X.; Seger, B.; Pedersen, T.; Yao, T.; Ding, C.; Shi, J.; Chen, J.; Li, C. Integrating a dual-silicon photoelectrochemical cell into a redox flow battery for unassisted photocharging. *Nat. Commun.* **2016**, *7*, 11474−11482.
(41) Rosso, K. M.; Smith, D. M. A.; Wang, Z.; Ainsworth, C. C.; Fredrickson, J. K. Self-exchange electron transfer kinetics and reduction potentials for anthraquinone disulfonate. *J. Phys. Chem. A* **2004**, *108*, 3292−3303.
(42) Aeschbacher, M.; Graf, C.; Schwarzenbach, R. P.; Sander, M. Antioxidant properties of humic substances. *Environ. Sci. Technol.* **2012**, *46*, 4916−4925.
(43) Pirbadian, S.; El-Naggar, M. Y. Multistep hopping and extracellular charge transfer in microbial redox chains. *Phys. Chem. Chem. Phys.* **2012**, *14*, 13802−13808.
(44) Orsetti, S.; Laskov, C.; Haderlein, S. B. Electron transfer between iron minerals and quinones: estimating the reduction potential of the Fe(II)-goethite surface from AQDS speciation. *Environ. Sci. Technol.* **2013**, *47*, 14161−14168.

https://dx.doi.org/10.1021/acs.est.9b07134
Environ. Sci. Technol. 2020, 54, 4131−4139

(45) Gorski, C. A.; Edwards, R.; Sander, M.; Hofstetter, T. B.; Stewart, S. M. Thermodynamic characterization of iron oxide-aqueous Fe^{2+} redox couples. *Environ. Sci. Technol.* **2016**, *50*, 8538−8547.
(46) Bauer, I.; Kappler, A. Rates and extent of reduction of Fe(III) compounds and O_2 by humic substances. *Environ. Sci. Technol.* **2009**, *43*, 4902−4908.
(47) Roden, E. E.; Urrutia, M. M. Ferrous iron removal promotes microbial reduction of crystalline iron(III) oxides. *Environ. Sci. Technol.* **1999**, *33*, 2492.
(48) Poggenburg, C.; Mikutta, R.; Schippers, A.; Dohrmann, R.; Guggenberger, G. Impact of natural organic matter coatings on the microbial reduction of iron oxides. *Geochim. Cosmochim. Acta* **2018**, *224*, 223−248.
(49) Kaiser, K.; Guggenberger, G. Mineral surfaces and soil organic matter. *Eur. J. Soil Sci.* **2003**, *54*, 219−236.
(50) Amstaetter, K.; Borch, T.; Kappler, A. Influence of humic acid imposed changes of ferrihydrite aggregation on microbial Fe(III) reduction. *Geochim. Cosmochim. Acta* **2012**, *85*, 326−341.
(51) Jones, A. M.; Collins, R. N.; Rose, J.; Waite, T. D. The effect of silica and natural organic matter on the Fe(II)-catalysed transformation and reactivity of Fe(III) minerals. *Geochim. Cosmochim. Acta* **2009**, *73*, 4409−4422.
(52) Nevin, K. P.; Lovley, D. R. Mechanisms for accessing insoluble Fe(III) oxide during dissimilatory Fe(III) reduction by Geothrix fermentans. *Appl. Environ. Microbiol.* **2002**, *68*, 2294−2299.
(53) Jiang, J.; Kappler, A. Kinetics of microbial and chemical reduction of humic substances: Implications for electron shuttling. *Environ. Sci. Technol.* **2008**, *42*, 3563−3569.
(54) Kappler, A.; Benz, M.; Schink, B.; Brune, A. Electron shuttling via humic acids in microbial iron(III) reduction in a freshwater sediment. *FEMS Microbiol. Ecol.* **2004**, *47*, 85−92.
(55) Wolf, M.; Kappler, A.; Jiang, J.; Meckenstock, R. U. Effects of humic substances and quinones at low concentrations on ferrihydrite reduction by Geobacter metallireducens. *Environ. Sci. Technol.* **2009**, *43*, 5679−5685.
(56) Sparks, D. L. *Environmental Soil Chemistry*; Academic Press: Boston, U.S.A., 2003.

https://dx.doi.org/10.1021/acs.est.9b07134
Environ. Sci. Technol. 2020, 54, 4131−4139